

Integration of direct air capture with Allam cycle: innovative pathway in negative emission technologies

Item Type	Journal article
Authors	Ghorbani, Alireza; Gharehghani, Ayat; Saray, Jabraeil Ahababi; Andwari, Amin Mahmoudzadeh; N. Borhani, Tohid
Citation	Ghorbani, A., Gharehghani, A., Saray, J.A., Andwari, A.M., Borhani, T.N. (2025) Integration of direct air capture with Allam cycle: innovative pathway in negative emission technologies. Energy Conversion and Management, 332, 119746.
DOI	10.1016/j.enconman.2025.119746
Publisher	Elsevier
Journal	Energy Conversion and Management
Download date	2026-05-20 19:20:51
License	https://creativecommons.org/licenses/by-nc-nd/4.0/
Link to Item	https://wlv.openrepository.com/handle/2436/626264

Integration of Direct Air Capture with Allam Cycle: Innovative Pathway in Negative Emission Technologies

Alireza Ghorbani^a, Ayat Gharehghani^{a,*}, Jabraeil Ahbabi Saray^a,

Amin Mahmoudzadeh Andwari^b, Tohid N. Borhani^c

^a School of Mechanical Engineering, Iran University of Science and Technology, Tehran, Iran.

^b Machine and Vehicle Design (MVD), Materials and Mechanical Engineering, Faculty of Technology, University of Oulu, FI-90014 Oulu, Finland.

^c Centre for Engineering Innovation and Research, School of Engineering, Computing and Mathematical Sciences, University of Wolverhampton, UK.

Abstract

The advancement of negative emission technologies (NETs) is crucial for addressing climate change by reducing atmospheric carbon dioxide levels. This study presents a comprehensive evaluation of a High Temperature Direct Air Capture (HT-DAC) system integrated with a supercritical CO₂ (S-CO₂) cycle, representing a significant advancement in carbon capture, energy optimization, and NET systems. Given to significant energy demands of HT-DAC, the primary objective of this research is to address the process's energy intensity by focusing on the development of a more efficient power island. Specifically, this study investigates the energy demands of the Air Separation Unit (ASU) to minimize energy consumption and improve the overall efficiency of the Allam cycle when coupled with the ASU. Additionally, the study examines the thermal integration of the system using pinch analysis to assess the impact of this innovative power island on energy efficiency. Key results indicate that the proposed system is capable of capturing 0.99 million tons of CO₂ per year directly from the air, achieving a capture efficiency of 75%. The specific energy requirement for the process is initially 3.19 kWh per kg of captured CO₂, which is reduced to 2.21 kWh/kgCO₂ following process optimization and heat integration. Through this optimization, hot and cold utility demands are reduced by 69.7% and 36.9%, respectively, while 110.1 MW of heat is recovered through the design of heat exchangers network, resulting in an 9.66% reduction in overall energy demand compared to the base case. Furthermore, the integration of captured and regenerated CO₂ (135.1 tons per hour with a purity of 98.1 mol%) offers substantial potential for synthetic fuel production and underground storage.

Keywords: Negative Emission Technologies; Direct Air Capture; Liquid Absorbent; Allam Cycle; Carbon Capture and Storage

Synopsis: This study demonstrates advancements in energy-efficient carbon capture through High Temperature Direct Air Capture (HT-DAC), reducing atmospheric CO₂ and supporting climate change mitigation.

* Corresponding Author:

Ayat Gharehghani, E-mail: Ayat_Gharehghani@iust.ac.ir, Tel: +98 21 73228953

1 Introduction

The Paris agreement has been proposed to hold temperature increment below 2°C pre-industrial levels and reach net-zero emissions until 2050 [1]. Green House Gases (GHGs) emissions should be reduced to a point in a balance with the amount of Sequestered ones and then make a ramp up for the sequestration of GHGs [2]. Mostly around 30-50% of global emissions are related to mobile sources which is still released to the air [3]. With increment in energy demand in the world the CO_2 concentration has raised to 414 ppm by 2019 [4, 5]. Negative Emission Technologies (NETs) can be considered the final option for reducing atmospheric CO_2 concentrations [6]. The concept of capturing CO_2 from atmosphere proposed by Lackner for reduction of climate change in 1990 [7]. Among the methods of capturing from distributed sources, Direct Air Capture (DAC) is one of the approaches for reaching to NET [8]. DAC systems to be able compete with other NETs need to be in gigaton-scale capture rate and should not be location dependent for their implementation and their cost must be reduced as low as \$100 and below for each tone of captured CO_2 [7, 9]. On the other hands capturing CO_2 from point sources classified in to three main technologies: post-combustion, pre-combustion and oxy-combustion [10]. The Allam cycle employs a novel approach by directly mixing oxy-fuel combustion byproducts into the working fluid, unlike conventional closed-cycle systems [11]. So for oxy-combustion cycles, interests in Supercritical Carbon Dioxide (S-CO_2) have increased recently [12]. According to Isles' research [13], the Allam cycle, a novel S-CO_2 cycle, eliminates the need for a steam Rankine cycle and enables a more efficient Brayton cycle. Allam-Fetved or NET power cycle is a high pressure, semi close, highly recuperative Brayton cycle with CO_2 mainly as a working fluid [14, 15]. Combination of these two types of carbon capture technologies (DAC and S-CO_2) can boost CO_2 removal from atmosphere while preventing further emissions. By increment in CO_2 capture, next question rise, what to do with this captured CO_2 . According to an estimation totally, 190 Gt CO_2 need to be stored. At 2020 capture capacity and storage has been around 40 Mt CO_2 per a year [16]. CarbFix claimed they can convert 95% of injected CO_2 in to minerals in less than 2 years [17].

Mature technologies for capturing CO_2 from air are High-Temperature Direct Air Capture (HT-DAC) and Low-Temperature Direct Air Capture (LT-DAC) which use liquid solvent and solid sorbent for capturing CO_2 respectively. Both of the mentioned technologies contain two cycles, one for capturing and the other one for regeneration of captured CO_2 from air [18]. LT-DAC technology is based on an adsorption process in which solid sorbents interact with CO_2 molecules through physical and chemical adsorption. Adsorption processes typically utilize highly porous materials with a large surface area, enhancing the efficiency of CO_2 capture. DAC adsorbents have classified into six categories: silica gel, metal oxides, metal-organic frameworks (MOF), carbon materials, zeolites, and polymers. These adsorbents can be either functionalized or non-functionalized [19]. Various DAC approaches like Pressure Swing Adsorption (PSA), Temperature Swing Adsorption (TSA) and Vacuum-Pressure Swing Adsorption (VPSA) exist for this purpose. Hybrid methods like VPSA or vacuum-temperature swing adsorption (VTSA) with multi-stage CO_2 have also achieved high-purity CO_2 in the final product along with efficient CO_2 recovery. Among these approaches, VPSA has gained attention due to its potential for energy-efficient CO_2 separation [20]. Additionally, several innovative systems have been proposed. For instance, the concept of a carbon pump has been integrated into multi-stage adsorption beds utilizing a TSA

cycle to evaluate energy efficiency[21]. The HT-DAC technology is inspired by the Kraft process in which caustic solutions are used [22]. The term "caustic" refers to strong bases, particularly alkalis. The main caustic solutions considered to those formed by sodium hydroxide (NaOH), potassium hydroxide, (KOH), or calcium hydroxide (Ca(OH)₂). The Kraft process is traditionally used in the paper industry, which using and recycling of sodium hydroxide solutions in this process can also be applied for CO₂ capture by some modifications [23]. HT-DAC technology employs a four-step process for the absorption and regeneration of captured CO₂, as depicted in Fig.1. The absorption cycle utilizes an air contactor unit while the regeneration cycle employs a pellet reactor, a slaker and a calciner [24]. For the regeneration cycle energy will be needed in order to separate CO₂ from calcium carbonate (CaO₃) which has been formed in pellet reactor [25].

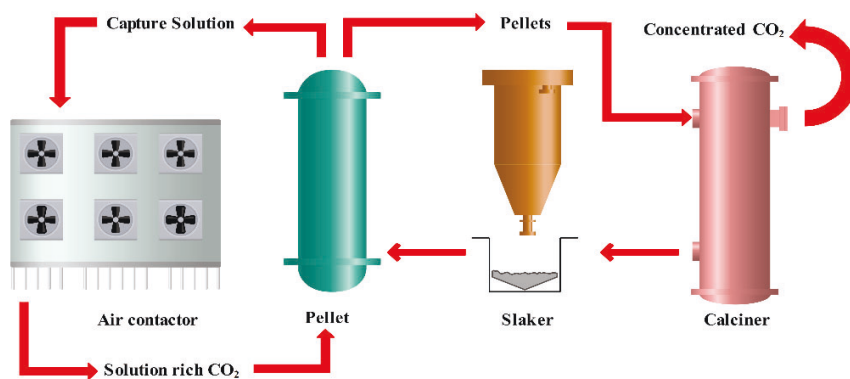


Fig.1 Schematic diagram of HT-DAC process

1.1 Literature review for HT-DAC

Zeman and Lackner [26], initially proposed the concept of capturing CO₂ from air through wet scrubbing using hydroxide solvents. This process is known as HT-DAC. They recommended employing NaOH as the liquid solvent and the Kraft process for recycling. The minimum net energy penalty was reported 2.6 GJ per ton of CO₂ captured from air. In the regeneration cycle of HT-DAC, CO₂ reacts with NaOH to form CaCO₃ pellets. the pellets are heated to a very high temperatures (around 900°C) to release CO₂ and regenerate CaO. Hence, the energy requirement is substantially high. Baciocchi et al. [27] further advanced this concept, providing the initial conceptual process design along with energy and mass balance assessments. They proposed two distinct process types. In their designs, the total energy demand was reported as 17 and 12 GJ per ton of CO₂ captured, respectively. Additionally, they recommended utilizing steam instead of water for the slaker of the process. Mahmoudkhani and Keith [28], described a method for recovering NaOH from sodium carbonate involving a titanate cycle. The primary advantage of the titanate cycle over traditional causticization is its lower operating temperature, approximately 50-100°C. Socolow et al.[29] reported that the net thermal energy requirement, assuming 75% thermal efficiency, was 8.1 GJ per ton of CO₂ captured, with an additional electricity consumption of 1.78 GJ/tCO₂. Their process utilized NaOH for CO₂ absorption, achieving a 50% capture rate. CO₂ was stored at a rate of 171 tons per hour. Ultimately, they provided a more realistic cost estimation for

CO₂ capture, ranging from \$430 to \$550 per ton. Mahmoudkhani et al. [30], investigated the utilization of a low-packed tower for CO₂ absorption from air, employing titanate compounds, and integrated it with a traditional lime cycle for the recovery process. They determined that 85% of the energy consumption in the packed columns was attributable to pump operation. By implementing a periodic pump operation with a 5% duty cycle, the energy required for fluid pumping can be reduced by about 90%. Keith et al. [31] incorporated KOH into their design to enhance uptake kinetics, opting for steam slaking instead of conventional slaking. The process achieves a CO₂ capture rate of 1 million metric tons per year. The air contactor achieves a CO₂ capture efficiency of 74.5% from the atmosphere. Meanwhile, the calciner, with a 98% CaCO₃ conversion efficiency, consumes 4.05 GJ/tCO₂. Their findings suggest that the levelized cost could potentially reach as low as \$94 per metric ton of CO₂. Sabatino et al. [32] investigated the application of bipolar membrane electro dialysis (BPMED) for the regeneration cycle to reduce the energy demand during the desorption process. Their study reported a capture cost of \$773 per ton of CO₂ and an energy requirement of 236 KJ/mol-CO₂, which is less energy-intensive compared to other methods. However, the cost still remains a significant challenge. Marchese et al. [33] conducted a comprehensive analysis of DAC for synthesizing Fischer-Tropsch (FT) fuels. In five different scenarios, they integrated a DAC unit with a hydrogen generation and a fuel synthesis unit. The efficiency of CO₂ capture varied from 58.1% to 68.2%, while the overall plant efficiency ranged between 22.6% and 36.5% [21]. Keju An et al. [34] proposed a method for modeling the air contactor in HT-DAC systems and examined how humidity and capture rate impact the energy requirements of a CO₂ capture plant. Their findings indicated that the energy demand could vary between 11.1 and 8.3 GJ per ton of CO₂ as the capture rate increased from 40% to 85%. Zolfaghari et al. [35] conducted simulations of CO₂ capture using HT-DAC technology and optimized the system's energy consumption. They reported an energy requirement of 343 kWh electricity and 5.24 GJ of heat per ton of CO₂ captured. Salvado et al. [18] examined a solar powered DAC and conducted a Life Cycle Assessment (LCA) to evaluate the environmental impact of their system. They found that the cost of solar-powered DAC ranged from \$260 to \$320 per ton of CO₂ captured.

1.2 Literature review for Allam cycle

Allam et al. [36] proposed an innovative oxy-fuel power cycle, asserting that the electricity cost of this new power cycle is highly competitive with existing ones. They reported cycle efficiencies of 59% and 51% for natural gas and coal respectively. Hervas and Petrakopoulou [10] conducted an exergoeconomic analysis of the cycle, reporting a net efficiency of 53.9% and an exergetic efficiency of 50.1%. They also determined the electricity cost to be 91.7 €/MWh. Zhu et al. [37] proposed a novel configuration of the Allam cycle, referred to as the Allam-Z cycle. In their study, they reduced the turbine inlet temperature and increased the turbine outlet pressure, using pumps rather than compressors to pressurize CO₂. The reported efficiency of the cycle was 48.05%. Sleiti and Al-Ammari [38] investigated various configurations of the Allam cycle, reporting a maximum thermal efficiency of 52% in their study. Additionally, they explored the integration of the S-CO₂ cycle with Concentrated Solar Power (CSP) [39]. Xin et al. [11] proposed a novel splitting analytical method and examined the impact of turbine cooling and recompression modifications on the cycle's efficiency and performance. Their results indicated that the optimized cycle

efficiency could reach 55.17%. Haseli and Sifat [40] reported an optimized cycle efficiency of 59.7% when incorporating a cryogenic Air Separation Unit (ASU). Given the critical role of the ASU, its thermal integration with the Allam cycle significantly impacts the cycle's performance. Therefore, the effect of compressor discharge pressure was also considered.

Fernandes et al. [41] investigated the process and carbon footprint associated with integrating the Allam cycle with an ASU and also conducted an exergy analysis. Within the ASU, the cryogenic heat exchanger exhibited the highest exergy destruction at 60.82%, followed by the main air compressor at 16.39%. In the Allam cycle, the combustor, recuperator, and turbine showed the highest exergy destruction, respectively. Colleoni et al. [15] conducted research indicating that Turbine Inlet Pressure (TIP) and Turbine Outlet Pressure (TOP) remain relatively constant around the point of maximum efficiency, whereas Turbine Inlet Temperature (TIT) is the most influential independent variable. Their results demonstrated that, without thermal recovery from the ASU, the net efficiency could reach up to 50.4%. Scaccabarozzi et al. [42] identified key factors impacting cycle efficiency, including the energy demand of ASU, cooling medium temperature, turbine cooling, and regenerator effectiveness. They later proposed integrating the Allam cycle with an upstream Solid Oxide Fuel Cell (SOFC), sending the exhaust gases to the combustion chamber for further combustion. This integration yielded an impressive net efficiency of 75.7% [43]. Chan et al. [44] conducted a parametric analysis of the Allam cycle integrated with a Liquefied Natural Gas (LNG) regasification process. Their study found that the highest exergy efficiency achieved was 50.31%, while the lowest product cost was \$1.654 per gigajoule. Meanwhile, there are several publications exploring the integration of the Allam cycle with various chemical processes. Wang et al. [45] suggested integrating the Allam cycle with an ASU and an ammonia production unit. Their analysis indicated the potential for achieving increased revenue per unit of natural gas consumption and lower CO₂ emissions compared to conventional ammonia plants. Xu et al. [46] explored the potential for polygeneration through the combined production of power and ammonia utilizing biomass. They integrated three subsystems to facilitate cascade heat utilization. In this configuration, CO₂ and H₂ are utilized for the Allam cycle and ammonia production, respectively. Xin et al. [47] examined the utilization of coal in the Allam cycle for polygeneration, focusing on methanol production. They conducted energy and exergy analyses of the proposed systems and reported an Allam cycle efficiency of 41.71%. The most recent study by Ioannou et al. [48] conducted a comparative analysis of life cycle and financial analysis across four scenarios aimed at producing valuable products from CO₂. They explored the integration of CO₂ capture from the air as a feedstock into a refinery plant. In one scenario, the utilization of residual gas in an Allam cycle was examined to improve the efficiency of the refinery plant.

1.3 Objectives and contributions of the study

Table 1 summarizes previous studies focused on capturing CO₂ from the air using various methods. This study introduces and evaluates a novel system for HT-DAC by integrating a S-CO₂ cycle, an approach not previously explored. The integration of the innovative S-CO₂ cycle with DAC technology offers a promising pathway to achieve NETs. Unlike earlier research, which examined areas such as the feasibility of CO₂ capture and heat management improvement [26], process design focusing on HT-DAC and NaOH absorption [27], and various techno-economic

assessments [31-33], this research provides a comprehensive model that integrates HT-DAC using KOH with the S-CO₂ cycle. By bridging these advanced technologies, this study makes a significant contribution to the field of carbon capture and energy optimization, marking a substantial advancement in the development of efficient NETs.

The significance of HT-DAC lies in its ability to capture CO₂ directly from the air, offering an effective solution for reducing greenhouse gas concentrations. On the other hand, the S-CO₂ cycle is recognized as one of the most advanced energy production technologies, known for its high energy efficiency and ability to operate at elevated temperatures and pressures. Integrating these two systems in this study not only optimizes energy consumption during CO₂ capture but also enhances overall process efficiency. This research addresses several key factors: the design of the ASU to meet the requirements of both the power cycle and the DAC cycle, evaluation of plant performance with the S-CO₂ cycle without reliance on conventional gas and steam turbines, and energy optimization using Pinch analysis to minimize the system's overall energy consumption.

Table 1. Overview of research on HT-DAC and the positioning of the present study.

Ref.	Objective of the study	Sub-systems			Description
		DAC	ASU	Allam Cycle	
Zeman, Lackner [26]	Feasibility of CO ₂ capturing directly from the atmosphere and the effect of heat management on process	✓	-	-	Based on absorption through hydroxides
Baciocchi et al. [27]	Process design of carbon dioxide capture from atmosphere	✓	-	-	Process, absorption by NaOH
Mahmoudkhani, Keith [28]	Thermodynamic analysis of the process	✓	-	-	NaOH recovery from an alkaline solution
Keith et al. [31]	Detailed techno-economic analysis for DAC plant for 1Mt capture	✓	✓	-	Absorption by KOH, combined cycle
Sabatino [32]	Evaluation of the energy requirements and costs associated with the process	✓	-	-	A novel DAC: wet scrubbing, BPMED for regeneration
Marchese et al. [33]	Evaluation energy and mass integration of DAC + FT process	✓	✓	-	DAC based on C.E, combined cycle
An et al. [34]	Impact of temperature and relative humidity of the air on the energy demand, CO ₂ capture efficiency, and the levelized cost of removal	✓	✓	-	Kinetic model for absorption, Scenarios with NGCC and grid connection
Prats-Salvado et al. [18]	Techno-economic and environmental assessment, including LCA, to compare the performance of solar powered HT-DAC	✓	✓	-	Liquid alkali solution, CSP for calciner heat demand

Current study	Performance assessment of HT-DAC with a S-CO ₂ cycle and optimization of its energy consumption	✓	✓	✓	Using KOH, S-CO ₂ cycle, cryogenic ASU
---------------	------------------------------------------------------------------------------------------------------------	---	---	---	---------------------------------------------------

2 Methodology

The absorption process can be conducted using either physical or chemical solvents in continuous operation. Chemical sorbents, unlike physical sorbents, demonstrate superior CO₂ absorption efficiency and selectivity, particularly at lower concentrations[49]. The selection of the absorbent in process design significantly influences both the amount of CO₂ absorbed and the energy consumption of the process. Alkaline solutions are effective for capturing dilute CO₂ from the atmosphere due to their relatively fast absorption kinetics, despite their highly corrosive nature. For absorption by solvents, alkaline hydroxides such as NaOH and KOH are utilized. These solvents, characterized as light hydroxides, chemically react with CO₂ to form carbonates. In this study, KOH was employed for chemical absorption of dilute CO₂ from air, and the integration of three distinct subsystems was investigated. The simulated CO₂ capture process from air is based on HT-DAC process data provided by Carbon Engineering, currently undergoing commercial implementation [31].

The Allam cycle's production of nearly pure CO₂ eliminates the need for absorber columns in the power island section. This cycle uses S-CO₂ as the working fluid, providing high efficiency and facilitating carbon capture. One of the key advantages of the Allam cycle is its inherent capability for carbon capture, storage, or utilization. This feature makes the Allam cycle particularly suitable for integration with the regeneration cycle of HT-DAC technology, as it does not require additional processes to purify the generated CO₂ in the power generation cycle. Both the HT-DAC and Allam cycles require pure oxygen for their combustion processes (oxy-fuel combustion). The sensitivity of these combustion processes to the oxidant flow composition necessitates the use of an ASU that provides an oxidant stream free of components such as N₂, to prevent the formation of NO_x during combustion. Consequently, an ASU block has been developed for both subsystems, based on Zolfaghari's ASU block simulation [35]. More details are available in section 2.2.

2.1 Chemical reactions and thermodynamic models

The chemical reactions for the HT-DAC section are outlined in Table 2. These reactions, which include the ionic components, are generated by the electrolyte wizard of Aspen Plus as equilibrium, dissociation, and salt formation reactions. The coefficients for the chemical equilibrium constants are obtained from the Aspen Plus databank. The remaining reactions within the process are specified in their respective sections, such as the slaker, calciner, and combustion chamber. Further details regarding these reactions will be provided in the subsequent process sections.

Table 2. Chemical reactions for the HT-DAC process.

	Reaction	Type
(1)	$2\text{H}_2\text{O} \leftrightarrow \text{OH}^- + \text{H}_3\text{O}^+$	Equilibrium
(2)	$2\text{H}_2\text{O} + \text{CO}_2 \leftrightarrow \text{HCO}_3^- + \text{H}_3\text{O}^+$	Equilibrium
(3)	$\text{H}_2\text{O} + \text{HCO}_3^- \leftrightarrow \text{CO}_3^{2-} + \text{H}_3\text{O}^+$	Equilibrium
(4)	$\text{CaOH}^+ \leftrightarrow \text{Ca}^{2+} + \text{OH}^-$	Equilibrium
(5)	$\text{CaCO}_3 \leftrightarrow 2\text{CO}_3^{2-} + \text{Ca}^{2+}$	Salt
(6)	$\text{K}_2\text{CO}_3 \leftrightarrow 2\text{K}^+ + \text{CO}_3^{2-}$	Salt
(7)	$\text{Ca}(\text{OH})_2 \leftrightarrow \text{CaOH}^+ + \text{OH}^-$	Dissociation
(8)	$\text{KOH} \leftrightarrow \text{OH}^- + \text{K}^+$	Dissociation

This simulation consists of three main different blocks with different thermodynamic properties. For DAC block thermodynamic properties were estimated by ENRTL-RK for liquid phase, RK-SOAVE and Henry's Law for the gas phase and Steam-NBS equation of state (EOS) for steam in HT-DAC block. For the Allam cycle and the Air Separation Unit of the process SRK and Peng Robinson EOSs were used respectively. The process simulated by Aspen PlusTM software (V11). Mass and energy balance and thermodynamic transformation of streams were obtained by it.

2.2 Process layout

This process comprises three primary blocks (see Fig. 2). In this work in compliance with Carbon Engineering HT-DAC process, fuel is supplied to the calciner reactor of the HT-DAC to fulfill its thermal requirements. However, the Allam cycle has replaced the traditional combined power cycle with carbon capture to meet the electrical demands of the HT-DAC and ASU subsystems. The ASU section consumes electricity to operate equipment such as compressors and pumps, and produces the oxygen needed for both the Allam cycle and the calciner of the HT-DAC block. For this purpose, cryogenic process is the most efficient and cost-effective method for producing oxygen both in gas and liquid phases. It uses a two-column cryogenic distillation method for high recovery and purity of oxygen from compressed air. The air is first pretreated to remove contaminants, then cooled to cryogenic temperatures to separate the gases and finally pressurized it to the required final pressure. This unit is important in two aspects: power consumption and the provision of high-pressure, high-purity oxygen. The HT-DAC block consumes electricity and fuel for CO₂ capture and regeneration of it. In this process simulation, the HT-DAC absorption cycle was designed to achieve a 75% CO₂ capture efficiency. Beyond carbon capture, this integration also facilitates water production within the Allam and ASU blocks.

The simplified process flow diagram (PFD) for the described sections is illustrated in Fig. 2. In this figure solid, liquid and gas streams are represented by black, blue and orange colors respectively. The process comprises three main blocks: HT-DAC, the Allam cycle, and the ASU.

Within the HT-DAC block, delineated by a black dashed line, there are five additional sub-blocks. Air contactor, Pellet reactor, Steam slaker, Calciner and CO₂ Compression unit.

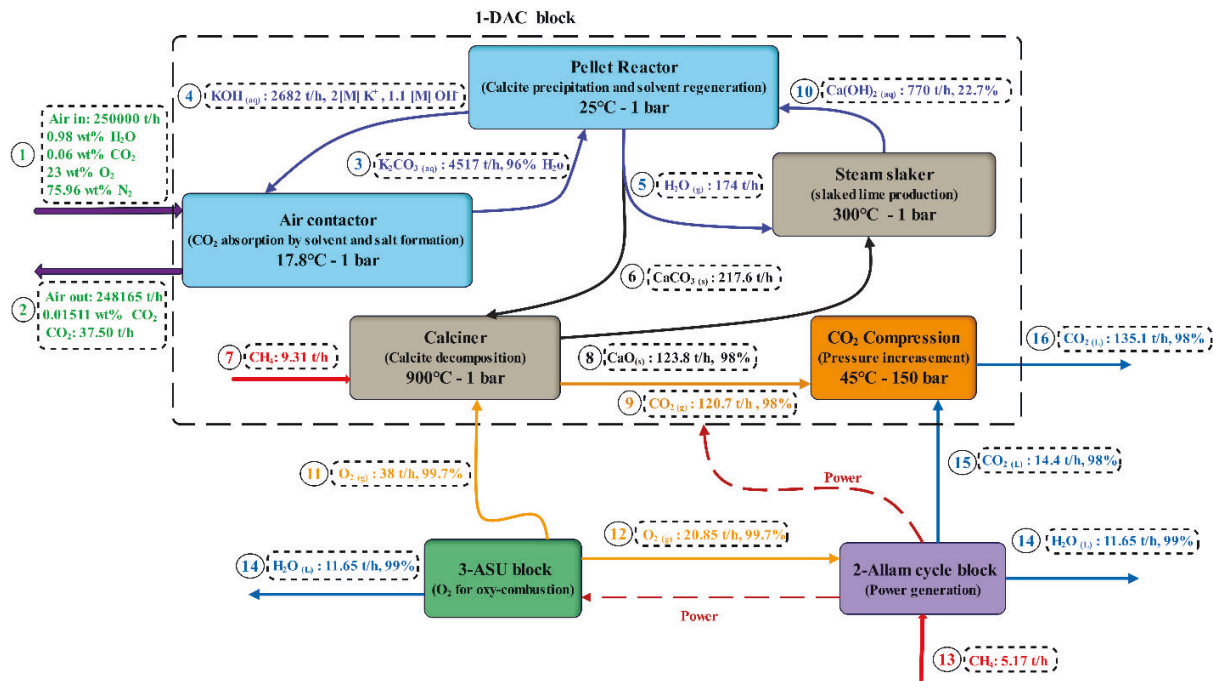


Fig. 2 Schematic overview of process integration for this study

In HT-DAC process, dilute CO₂ from atmosphere (0.06 wt %) is captured using an aqueous KOH solution in the air contactor, and then directed to pellet reactor (St. 3). In the pellet reactor, solid calcite precipitates and is subsequently transferred to the calciner (St. 6). During this process, KOH is regenerated and returned to the air contactor (St. 4) to ensure continuous operation of the HT-DAC absorption cycle. The calciner's energy demand is met through fuel injection (St. 7). The calciner's products are then routed to the steam slaker (St. 8) and the compression unit (St. 9). Concurrently, vaporized water (St. 5) from the pellet reactor is sent to the steam slaker, where it reacts with CaO from the calciner to produce Ca(OH)₂ (St. 10), which is returned to the pellet reactor for regenerating the aqueous solution.

The ASU block is responsible for supplying oxygen. Oxygen is delivered to the calciner (St. 11), while St. 12 is directed to the Allam cycle for oxy-combustion in the power generation block. The produced CO₂ by Allam cycle (St. 15) is already at high pressure and does not require additional compression. This CO₂ is combined with the regenerated CO₂ from the HT-DAC calciner (St. 9), resulting in St. 16. Another benefit of the Allam cycle is its capability to produce water (St. 14), which can reduce the water consumption of the HT-DAC process. In power generation cycle fuel is injected with St. 13. The generated power is supplied to both the HT-DAC and ASU blocks via power streams represented by a red dashed line. The process is on steady state condition and for all sections pressure loss is neglected. The impact of emissions leakage is not considered, and it is assumed that the Allam cycle achieves 100% CO₂ capture. Additional assumptions are detailed in the process layout sections.

2.2.1 Allam cycle

Table 3 summarizes the input parameters used for the depicted Allam cycle block in Fig. 3. In this section, no heat losses were considered, and the mechanical efficiency of the equipment was assumed to be 100%. In this simulation pure methane is assumed instead of natural gas. The methane is compressed (St.1) using two-stage compressors with an intercooler, achieving a final temperature of 151°C and a pressure of 30 MPa. Subsequently, this methane is combusted with recycled CO₂ and oxygen supplied from the ASU block.

Table 3. Input parameters summary for the Allam cycle [50].

Item	Value
Compressors isentropic efficiency (%)	85
CO ₂ turbine isentropic efficiency (%)	85
Pumps hydraulic efficiency (%)	80
CO ₂ turbine pressure ratio	0.1
CO ₂ compressors pressure ratio	1.45

Combustion occurs in a constant pressure and adiabatic environment, ensuring complete combustion of the fuel. The combustion is occurring with 0.5% excess oxygen. Oxygen required for the power island is supplied by the ASU section (St. O₂ ALLAM), with a purity of 99.7 mol %, delivered in vapor phase at 50°C. This oxygen stream is preheated by a recuperator (REC1) and then injected (St. 18) into the combustion chamber to complete the combustion process and close the cycle. The reaction products (St. 3), after expanding in the turbine, reach a temperature of 771°C. The hot stream exit temperatures for the first and second recuperators (REC1 and REC2) are 87°C and 67°C, respectively. Pressure loss in the recuperators during heat transfer is negligible. In St. 7 at 21.8°C, a flash separator (SEPARAT) separates water from CO₂, which is then sent for further compression. This process produces 11.61 ton/hr of liquid water with a purity of 99.6 mol %. Subsequently, the CO₂ stream (St. 10) undergoes four-stage compression with intercooling, achieving a pressure of 13.3 MPa and a temperature of 45°C in St. 11, with the liquid phase present. This stream is then divided into two separate streams, St. 12 and St. 14, using a splitter (SPILIT1). In St.12, 14.37 ton/hr of the main St. 11, which has a flow rate of 410.5 ton/hr, is separated for further sequestration or utilization and sent to the HT-DAC section. Here, it mixes with CO₂ regenerated from the calciner to enhance CO₂ sequestration capacity. After the splitter, St. 14 is directed to pump trains to increase its pressure to 30 MPa, with intercoolers maintaining the temperature at 51°C. Finally, St. 15 delivers liquid CO₂ to REC2 at 56.4°C, subsequently entering the combustion chamber at 676°C. St. 12 passes through the heat exchanger (COLLER2) and is cooled to 26.7 °C. This results in St. 13, which transports liquid-phase CO₂ to the HT-DAC block. Concurrently, the separated water, after exchanging heat with St. 12, reaches a temperature of 35.7 °C. For the overall system, the net electrical power of the Allam cycle can be calculated by Equation (1) [1].

$$\dot{W}_{net} = \dot{W}_T - \sum_0 \dot{W}_{Pump} - \sum_0 \dot{W}_{Comp} - \dot{W}_{ASU} \quad (1)$$

\dot{W}_{net} net is the net power output of this system that is equal to the sum of the power outputs of the CO₂ turbine minus the sum of the power consumptions of all the turbomachines and ASU. \dot{W}_{ASU} is the power output of expander minus the sum of the power consumptions of all the turbomachines of ASU block. This power demand has been calculated by Equation (2) [1].

$$\dot{W}_{ASU} = \dot{W}_{T,ASU} - \sum_0 \dot{W}_{Pump,ASU} - \sum_0 \dot{W}_{Comp,ASU} \quad (2)$$

For efficiency calculation of cycle as shown in Equation (3) [1], \dot{m}_{fuel} represents the mass flow rate of injected fuel to the cycle and LHV shows its heating value and \dot{Q}_{in} is showing amount of the heat is added to the system through hot utilities.

$$\eta_{tot} = \frac{\dot{W}_{net}}{\dot{m}_{fuel} \cdot LHV + \dot{Q}_{in}} \quad (3)$$

It's also notable that \dot{W}_{net} is the net power output that satisfies the power demand of the HT-DAC block. Figure 4 presents the P-H diagram of the Allam cycle integrated with HT-DAC and ASU. This diagram depicts the operating pressure, enthalpy, and temperature range of the power generation unit. For this diagram, CO₂ is assumed to be a pure gas. The saturation dome is shown in green, while the red lines represent the cycle processes, emphasizing the supercritical state of the Allam cycle's working fluid. As illustrated, the system employs a four-stage compression for CO₂ compression and a four-stage pumping process for liquid CO₂.

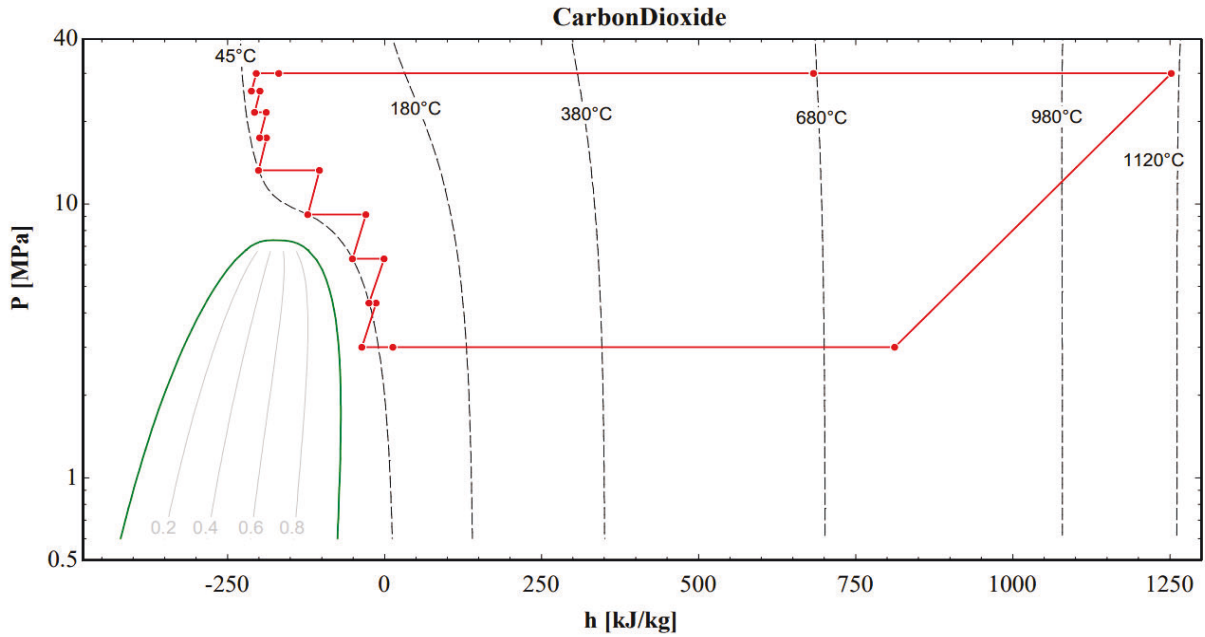


Fig. 4. Pressure-Enthalpy diagram of the Allam cycle integrated with the HT-DAC

2.2.2 Air separation unit

Fig. 5 presents a detailed process flow diagram of the ASU block. The input parameters utilized for simulating this block are outlined in Table 4. Within this block, atmospheric air at 21°C undergoes moisture removal prior to being subjected to multi-stage compression, which elevates the air pressure from atmospheric levels to 0.58 MPa.

Table 4. Input parameters of the ASU block [35].

Item	Value
compressors polytropic efficiency (%)	80
Expander polytropic efficiency (%)	80
Pump hydraulic efficiency (%)	80
Air compressors pressure ratio	1.8
HPC reboiler reflux ratio	0.9

The moisture content of air is ultimately separated using an adsorption unit. Following this, St. 54 is split into two separate flows. One of these flows, comprising 0.25% of the main stream's mass flow rate (St. 55), is routed to the expander (EXP-01), leading to a temperature of -54.5°C. The second stream, at a temperature of 35.1°C and a pressure of 0.58 MPa, is routed directly to a heat exchanger (HXE). St. 54 feeds the high-pressure column (HPC), where its temperature is reduced to -174°C. Concurrently, St. 59 reaches to -159.2°C and is directed into the low-pressure column (LPC). Liquid N₂ exits from the HPC at -177°C with a mass fraction of 97.2%, then passes through an expansion valve before entering the LPC at a pressure of 0.12 MPa. St. 62 also exits the HPC and, like the second stream, enters the LPC after passing through a valve. This stream enters tray 47 of the LPC, with the thermal requirements of the LPC's reboiler being entirely met by the heat rejected from the HPC's condenser. Eventually, St. 57 which is primarily liquid O₂ (99.7 wt%), and St. 58 which contains N₂ gas (92.8 wt%), pass through the heat exchanger (HXE), commonly known as the Cold Box. A portion of St. 57, designated as St. 57-1, with a mass flow rate of 58.85 ton/hr and a temperature of 35°C. It's directed to SP-02. Of this stream, 38 ton/hr of oxygen toward the DAC block, while the remainder is sent to the Allam cycle block for combustion. The O₂ gas is supplied to the Allam block at 0.13 MPa, necessitating a pressure increase. To mitigate the energy penalty associated with compressors throughout the system, it was decided to change the phase of the oxygen and then increase its pressure to 30 MPa. To accomplish this, a cooler (C-05) and a heater (H-01) were utilized to ultimately raise the oxygen temperature to 50°C at 30 MPa.

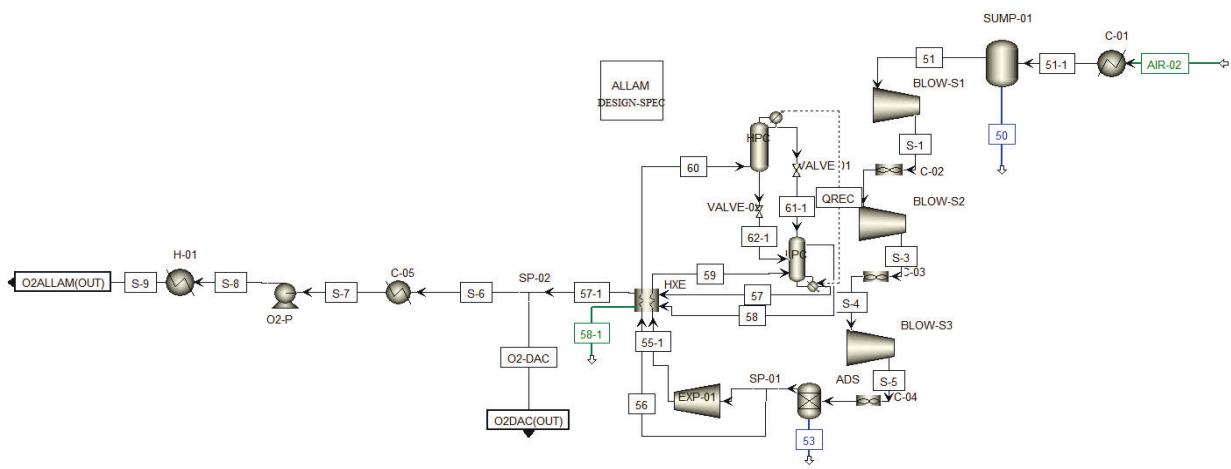


Fig. 3. Flow diagram of the ASU block process.

2.2.3 Direct air capture

The HT-DAC block consists of five sub-units: the air contactor, pellet reactor, calciner, steam slaker, and CO₂ compression unit. All five sections are integrated within the HT-DAC block. Fig. 6 illustrates all the mentioned sub-units of the HT-DAC block, with the air contactor serving as the core of the absorption cycle. The mentioned sub-blocks are depicted in Fig. 6 with violet dashed lines. In Aspen Plus, there is no specific block for simulating this process unit. To simplify the simulation, it has been modeled using two basic blocks: a mixer and a separator unit. This setup is designed to capture the incoming CO₂ from St.1, which has a mass flow rate of 250,000 ton/hr. The composition of the inlet air follows Keith's data [31]. The liquid solvent (St.3) enters the air contactor with molarities of 2 for K⁺, 1.1 for OH⁻ and 0.45 for CO₃²⁻. After the CO₂ is absorbed by KOH, the solution is sent to a pumping unit to counteract the pressure loss in the air contactor. Subsequently, the absorbed CO₂ begins to form dissociated potassium carbonate (K₂CO₃).

Pellet reactor is a crystallizer unit in which CaCO₃ begins to precipitate as a solid in St. 12. SEP-2, modeled as part of the pellet reactor, directs most of the solids to FILTER-3, while predominantly liquid components are sent to Filter-1 and Filter-2. At St. 24, containing CaCO₃ at 25°C is directed to the washer unit, where its exiting temperature is increased to 53°C (St.29). For maximum heat recovery, Ca(OH)₂ product from the steam slaker (SLAKR) is integrated with St. 29. Ultimately, this stream's temperature is increased to 300°C, converting the liquid water into superheated steam by heaters. In the SP-4 block, steam and solid CaCO₃ are separated, with the steam being routed to the slaker unit and solid CaCO₃ directed to the calciner unit. The solid CaCO₃ enters the calciner block at 464°C, where 98% of it decomposes into CaO and CO₂. This block operates at 900°C, a temperature maintained by oxy-combustion of fuel within the calciner. In the SEP-3 block, the gas and solid streams are separated, with the gas stream sent to the CO₂ compression section and the solid stream directed to the slaker reactor section. Solid CaO reaches a temperature of 674°C before entering the steam slaker. The SLAKR reactor operates at 300°C, converting 85% of St. 62-1 to Ca(OH)₂. Water enters the slaking section to meet the reactor's return flow requirements. This water is pressurized to 42 bars by PUMP-4 and mixed with the return flow at 50°C (St.56). The remaining water is directed to heat exchangers and coolers to utilize its rejected heat.

The gas products from the calciner (St.41), after a water spray in SEP-5, are sent to a four-stage compression unit to achieve 45°C and 150 bar. Finally, the regenerated CO₂ by the HT-DAC and produced by the Allam cycle are combined in a mixer, resulting in a stream at 39°C and 120 bar with a mass flow rate of 133.7 ton/hr, ready for storage and sequestration.

2.3 Key performance indicators

Key Performance Indicators (KPIs) are established to assess the performance of the entire integrated plant. One KPI is the specific energy consumption of the plant, measured in relation to the amount of CO₂ removed from the air. This indicator reflects the energy required to capture CO₂. The formula for this KPI is presented as follows [33]:

$$E_{sp\ CO_2} = \frac{\dot{m}_{fuel} \cdot LHV_{fuel} + \dot{W}_{elec} + \dot{Q}_{th}}{\dot{m}_{CO_2\ cap}} \quad (4)$$

$$\dot{m}_{CO_2\ cap} = \dot{m}_{CO_2, Air\ in} - (\dot{m}_{CO_2, Air\ out} + \dot{m}_{CO_2, EXH\ out}) \quad (5)$$

Where \dot{m}_{fuel} is mass flow rate of fuel, $\dot{m}_{CO_2\ cap}$ is mass flow rate of captured CO₂ and $\dot{m}_{CO_2, Air\ in}$ is mass flow rate of CO₂ in the air entering absorption unit while $\dot{m}_{CO_2, Air\ out}$ is mass flow rate existing absorption unit. The \dot{W}_{elec} and \dot{Q}_{th} are electricity input and heat input of the whole plant respectively. Another KPI is efficiency of CO₂ removal from air. This KPI indicates how much the plant is efficient and suitable for capturing CO₂ from atmosphere and it's described as below:

$$\eta_{CO_2} = \frac{\dot{m}_{CO_2, Air\ in} - (\dot{m}_{CO_2, Air\ out} + \dot{m}_{CO_2, EXH\ out})}{\dot{m}_{CO_2, Air\ in}} \quad (6)$$

2.4 Thermal integration

Exploring all possible avenues to reduce energy consumption and associated costs underscores the importance of process integration strategies. Such approaches aim to maximize heat recovery, thereby minimizing the reliance on external heat sources and enhancing the overall thermal efficiency within the process. To achieve this goal, a calculation tool known as pinch analysis has been employed. The core of this approach is the strategic deployment of heat exchangers, which facilitate the recovery of thermal energy from hot process streams and the subsequent transfer of that heat to colder streams. This enables a more efficient utilization of the available thermal resources within the system. The integration process leveraging this method comprises two main steps: targeting and design. The targeting step identifies the optimal heat recovery opportunities, while the design phase focuses on configuring the heat exchange network to realize these opportunities. During the analysis, various graphical representations are generated to visualize and evaluate the heat recovery potential. For example, external cooling and heating requirements can be determined using Composite Curves (CC). Similar insights can be gained from the Grand Composite Curve (GCC). In GCC we can also identify possible integration of the proposed process. In this design, the Maximum Energy Recovery (MER) method is used to minimize the utility demand of the process. Theoretically, one can calculate the minimum possible requirement

for external heat or cooling sources for a heat exchanger network. Aspen Energy Analyzer software (V11) is utilized for targeting and integration analysis of the process.

Conversely, the optimal design for the heat exchanger network can be achieved by evaluating both the amount of energy recovered and the associated costs of that recovery. By utilizing the total cost target and identifying the appropriate minimum temperature difference (ΔT_{\min}), the minimum cost configuration can be determined. The capital cost of heat exchangers is calculated as demonstrated in Equation (4).

$$\text{CapitalCost (s)} = a + b \left(\frac{A}{N_{\text{shells}}} \right)^c \times N_{\text{shells}} \quad (7)$$

In this equation, A represents the targeted area of the network, and N_{shells} denotes the number of targeted shells. The constants a, b, and c are related to construction and material costs, with default values in the software set to $a=1000$, $b=800$, and $c=0.8$. The analysis is conducted over a 5-year period with a 10% rate of return (ROR) on the investment. In Fig. 7, the optimal ΔT_{\min} is plotted. This diagram graphically represents the relationship between the minimum operating temperature of a heat exchanger network and its total cost index. It follows a nonlinear trend, where a slight decrease in the minimum temperature initially leads to a modest cost reduction, but beyond a certain point, the total cost rises sharply. For this process integration, the selected ΔT_{\min} is 4°C . At the optimal temperature ($\Delta T_{\min} = 4^{\circ}\text{C}$) the capital cost is \$7.83 million, with an operating cost of 0.157 cost/s, resulting in a total cost index of 0.223 cost/s. As ΔT_{\min} increases, the operational cost also rises, thereby increasing the heat demand of the process.

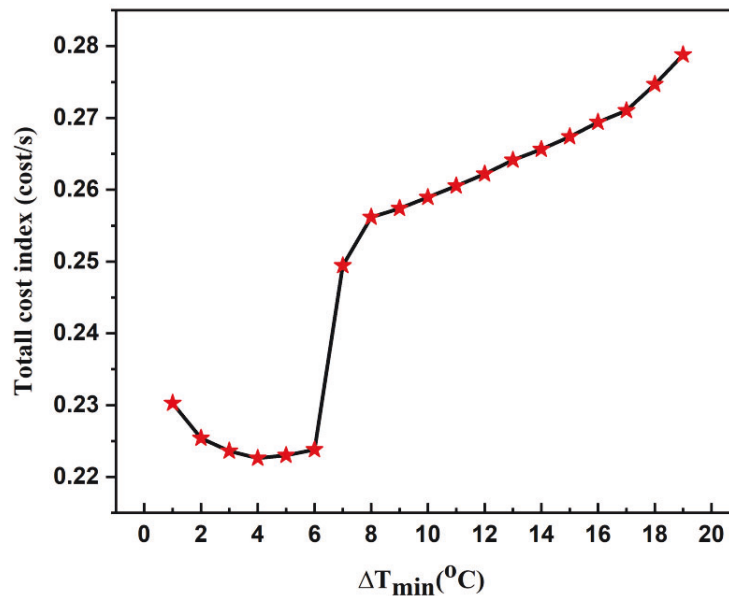


Fig. 5. Determining the lowest optimal temperature.

Considering the minimum temperature difference ΔT_{\min} constraint for the process means that a temperature difference lower than this allowable limit between the hot and cold streams is not permitted during the design stage. Once the optimal ΔT_{\min} has been determined for the simulated problem, all hot and cold streams can be visualized together in a single plot known as the CC. Fig. 8 illustrates the heat demand, heat removal, and thermal flux recovered by the proposed system. The minimum distance between hot and cold streams in this graph is known as the process pinch point. Overlapped section to the right of this point signifies the heat demand of the process, which must be met by the hot utility (47.87 MW), while the section to the left is referred to as the cold utility (64.60 MW). In this diagram, the minimum heat supply is represented by a violet two-sided arrow, while the minimum heat removal is indicated by a brown two-sided arrow. The recovered thermal flux is shown using a green arrow. This plot provides a graphical representation of hot and cold utilities, as well as the recovered heat. To precisely locate the pinch point and determine the potential for heat recovery, another graph known as the Grand Composite Curve (GCC) is required. This diagram is depicted in Fig. 9.

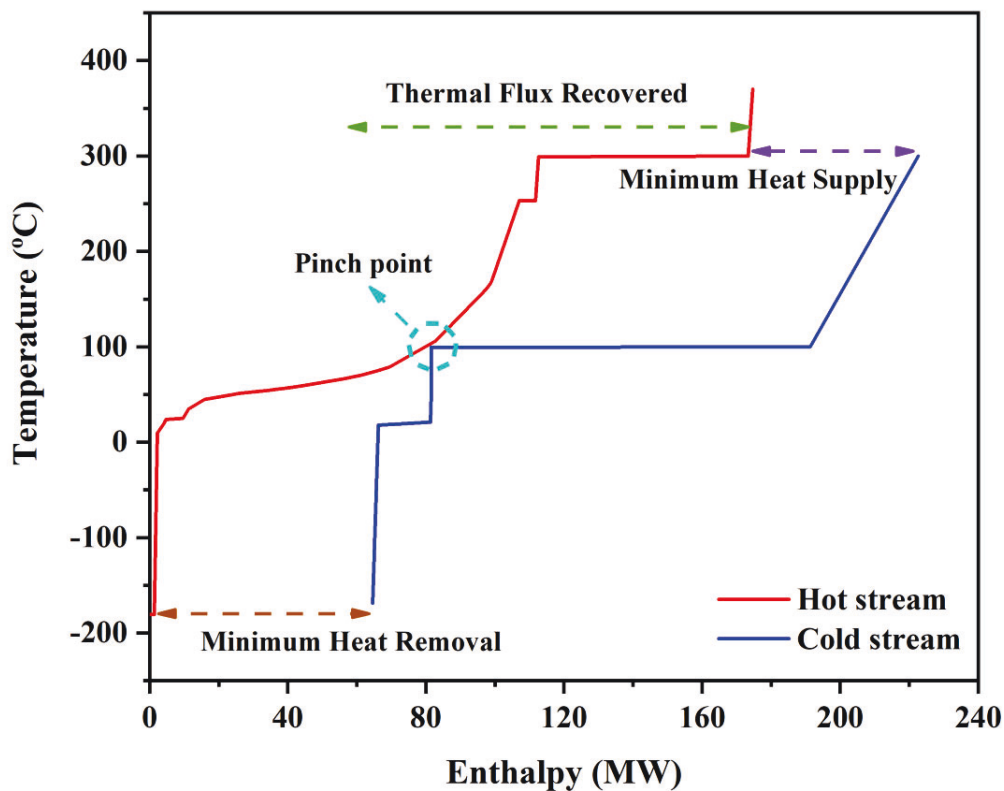


Fig. 6. Representation of the Composite Curve diagram for the heat exchangers network.

In the GCC, all hot and cold streams are plotted on a single curve, and the point where it intersects with a vertical line (at 101.7°C, the shifted temperature) indicates the pinch point location of the

process. Subsequently, the hot and cold shifted temperatures can be calculated by adding or subtracting ($\mp T_{\min}/2$). GCC diagram serves as a key tool in identifying the optimal locations and temperature levels for utility integration, minimizing external energy consumption while maximizing heat recovery. The regions above the pinch temperature indicate where external hot utilities are required, while regions below the pinch highlight the demand for cold utilities. The overlapped areas between hot and cold streams are often referred to as pockets. pockets indicate areas where internal heat exchange can take place without the need for external utilities. The larger the pocket, the greater the opportunity for energy savings and process efficiency improvements.

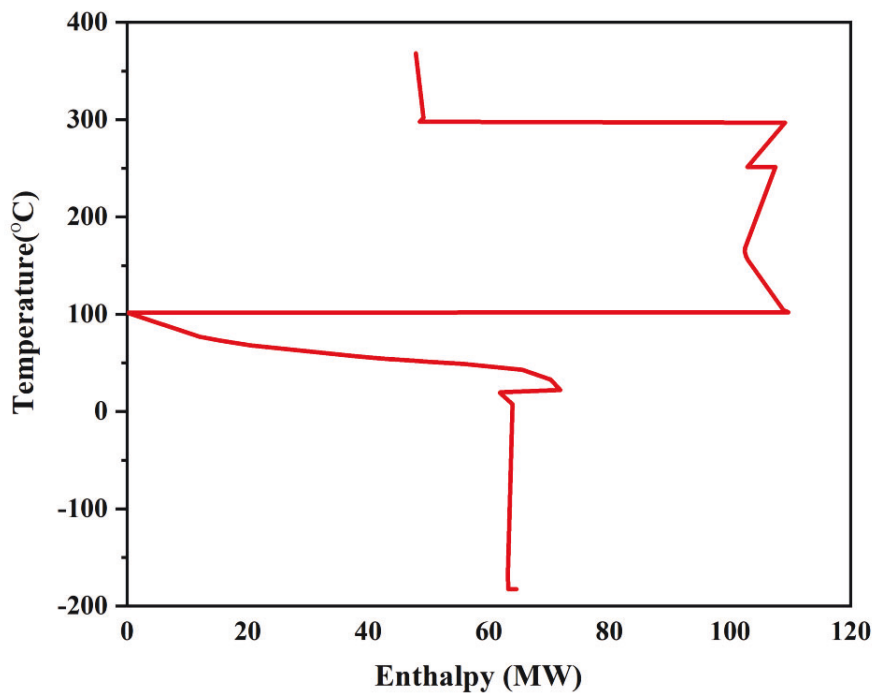


Fig. 7. Representation of the GCC diagram for the heat exchangers network.

3 Results and discussion

The primary objective of this research has been to optimize and improve the performance of the DAC plant. Undertaking this research endeavor, power unit of the DAC facility - as previously proposed by Keith [31], has been substituted with a novel and advanced cycle capable of capturing 100% of the CO₂ emissions. This innovative direct-fired S-CO₂ cycle, known as the Allam cycle, is capable of producing high-purity CO₂ as its output. Initially, simulations of the Allam cycle and its integration with the ASU were conducted. The ASU is crucial for both the DAC and Allam cycle processes. Modifications were made to the end section of the ASU due to the outlet temperature and pressure of the oxygen, ensuring it is compatible with the Allam cycle. Four distinct simulations were executed for this scenario. In one simulation, the oxygen pressure was

increased to 300 bar using four-stage compressors, while the other three simulations involved pumping liquid oxygen with one to three-stage pumps. The results indicated that four-stage compression resulted in cycle efficiency of 51.2%, whereas multi-stage pumping achieved an efficiency of 55.5% without significant variation. Consequently, following the principle of minimizing equipment use, only a single stage of oxygen pumping was considered. After identifying the best process for increasing oxygen pressure, all blocks were fully integrated, and the energy demand of the entire plant was assessed and optimized using the pinch analysis method as follows.

3.1 Validation

The Allam cycle modeled in this research was compared with the studies of Sifat and Haseli [51] and Sleiti et al. [52] as presented in Table 5. For this comparison Equations (1) and (2) are used for net power demand and ASU demand and Equation (3) has been utilized for efficiency calculation. In this study, with the same fuel mass flow rate and a Lower Heating Value (LHV) of 50 MJ/kg for methane, resulting in a net power output of 436.8MW. The CO₂ turbine in the cycle was modeled as a single stage, maintaining the same operating pressure as reference cases, resulting in a power output of 617.9 MW. Compared with two other cases, this study's recycled CO₂ flow rate is lower, with 43.1 kg/s of CO₂ exiting the cycle for storage, while 34.8 kg/s of water with 99.8 mol% purity is separated. No compressor unit was used for pressurizing oxygen, which impacts the cycle's efficiency. This process also required 11.97 MW of external heat, determined after heat integration and a pinch analysis. Additionally, the heat rejected from the HPC was integrated with the LPC's heat demand (29.16 MW) to reduce external heat requirement.

Ultimately, the model's efficiency calculated in this study was 55.5%, which is 9.3% higher than report of Sifat and Haseli [51] and 7.1% higher than report of Sleiti et al. [52]. As noted, the net output power of this study is greater than two other cases, resulting in a higher efficiency. This difference is attributed to the power of the fuel compressors, oxygen compressors, CO₂ compressors, and oxygen pumps. Despite the improvements achieved in the Allam cycle model, the efficiency reported by Allam [36] (59%) remains 6.3% higher than this proposed cycle configuration.

Table 5. Allam cycle comparative analysis results.

Parameters	Unit	[51]	[52]	This study
Fuel flow rate	kg/s	15.5	15.5	15.5
Oxygen flow rate	kg/s	63	62	62.31
Fuel temperature before combustor	K	493	461	417.2
Combustor Pressure	bar	300	300	300
Turbine inlet temperature	K	1423	1423	1423
Turbine outlet Pressure	bar	30	30	30

Turbine exhaust temperature	K	1068	1053	1027.7
Recuperator outlet temperature for combustion	K	336	350.1	339.6
Recuperator outlet temperature for CO ₂ recycled	K	1011	996	941.3
Recuperator inlet temperature for CO ₂ recycled	K	352	299	329
Flow rate of sequestrated CO ₂	kg/s	55	42	43.1
Flow rate of Recycled CO ₂	kg/s	1264	1200	1068.7
Turbine power	MW	640	622	617.9
Turbine efficiency	%	95	95	95
Compressor efficiency	%	95	95	95
Pump efficiency	%	95	95	95
ASU power	MW	70	84	70.4
Fuel Compressors power	MW	8	7	6.61
O ₂ Compressors power	MW	12	27	-
CO ₂ Compressors power	MW	83	72	76.9
CO ₂ pumps power	MW	51	31	27.2
NET output power	MW	393	401	436.8
NET efficiency (LHV)	%	50.78	51.8	55.5
Difference in efficiency	%	9.3	7.14	-

The ASU block used in the simulation was evaluated in comparison to the work of Zolfaghari et al. [35]. They modified their ASU block for integration with DAC to produce purified oxygen, thereby reducing the energy demand of the CO₂ compression unit in the DAC block.

Table 6. ASU performance comparison results.

	Unit	BLOW-S1	BLOW-S2	BLOW-S3	EXP-01
Zolfaghari et al. [35]	MW	3.993212	4.35282	4.351103	-1.34498
Present study	MW	3.993832	4.354144	4.352735	-1.34498
Difference	%	0.0155	0.0304	0.0375	0.0003

The power demand and production results of this ASU block are compared with the base case, as detailed in Table 6. In this validation process, 4.82 MW of heat rejected from the HPC was completely integrated with the LPC. Additionally, the system produced 37.1 ton/hr of oxygen, demonstrating compliance with the results of the reference model.

3.2 Mass balance

Using the environmental conditions as referenced in Keith et al. [31], 150 ton/hr CO₂ enters the air contactor unit, and 75% of this CO₂ is captured. For this capture mass flow rate of Air contactor solvent was varied by a design spec in order to get to desired capture rate which match with [33] (2681.6 ton/hr). In this process simulation, approximately 0.99 MtCO₂/year is captured through the HT-DAC absorption cycle. In the absorption cycle, reactions (1)-(3) occur, while the dissociation reaction (6) takes place, leading to the production of K₂CO₃ in its dissociated form in water. The absorbed CO₂ by solvent precipitated in the pellet reactor, producing CaCO₃ at a flow rate of 217.6 ton/hr, which was then sent to the calciner for CO₂ regeneration. Compared to Keith's data [31], where 300 ton/hr of CaCO₃ was precipitated, this investigation precipitated 27.5% less calcium carbonate. For the precipitation of the CaCO₃ in this simulation chemistry calculation method of crystallizer block has been utilized. This calculation method was implemented due to a lack of information on solubility data. Filters with fraction of solids to solids 1 have been used to separate solid particles from liquids. Precipitated CaCO₃ passed through a washer to separate impurities from CaCO₃ pellets. For this purpose, 551.4 ton/hr of water was utilized. A portion of this stream comes from water condensed in block SEP-5. In the calciner, 9.31 ton/hr of methane were completely combusted to generate the required heat to decompose 98% of the CaCO₃, producing 119.5 ton/hr of CaO, which was then directed to the slaker unit after the separation of solids and gas-phase materials. In order to have an adiabatic reactor at 900°C another design spec was considered for calciner to minimize fuel consumption. In the slaker unit, which is a fluidized bed reactor, the produced quicklime (CaO) reacted with steam at 300°C to form slaked lime (Ca(OH)₂). In this reactor, only 85% of the CaO was converted into Ca(OH)₂. The benefit of a steam slaker in this process is the release of reaction heat at high temperatures. The dust collector of the slaker unit separates solid CaO at a rate of 17.63 ton/hr for disposal. Table 7 provides a simplified overview of the key streams from the process simulation.

Table 7. Mass balance evaluation of the process.

Stream	Mass flow rate (ton/hr)
Air inlet	250000
Air outlet	248164.7
Air contactor solvent	2682.1
Water demand DAC	531
Slaker water demand	7
CO ₂ regenerated by DAC	119.5
CaCO ₃ entering calciner	217.6
Fuel to Calciner	9.31
ASU water separation	3.4
Air inlet to ASU	343.3

Water product of Allam cycle	11.6
CO ₂ product of Allam cycle	14.2
Fuel to Allam cycle	5.17

After the decomposition of CaCO₃ in the calciner, a flow of 141.1 ton/hr with 70 mol% CO₂ purity (St. 41) proceeds to the SEP-5 block. After water is removed by this block, 120.7 ton/hr of exhaust gases from the calciner, containing 98 mol% CO₂, are directed to the compression unit. To prevent water condensation in the compressors, the moisture content has been reduced by the water knockout block. This stream (St. 47) contains 0.81% oxygen and 1.1% moisture. To separate the moisture content in (St. 41), 531 ton/hr of water is used. Additionally, the slaker unit in the DAC block consumes 7 ton/hr of water, as determined by another design spec, to maintain 70.2 ton/hr of water in (St. 58-B) for continuous process operation.

In the ASU block, moisture is separated from the incoming atmospheric air and turned to water in two steps: the first step (SUMP-01) separates 0.38 kg/s of water, and the second step (ADS) separates 0.56 kg/s of compressed air. In total, 3.4 ton/hr of water is extracted from atmospheric air in the liquid phase. As mentioned earlier O₂ pressure need to rise from 1.3 bar to 300 bar for the combustion chamber of the Allam cycle, while the O₂ required for calciner does not need this pressure increasement. Separation of portion of the O₂ for pressure raise will avoid unnecessary power demand of ASU. For the pressure increasement by pump temperature has reduced from 35°C to -180.7°C. After pumping liquid O₂ to 300 bar its temperature from reached to 50°C by a heater. The produced O₂ is divided into two streams (SP-02), with 38 ton/hr sent directly to the DAC block and the remainder used in the Allam cycle. In this study, the oxygen flow rate to the calciner is higher than in the work by Zolfaghari et al.[35], resulting in a higher energy demand in the CO₂ compression unit for this research. In this study, the total mass flow of fuel (methane) is 14.48 ton/hr, with 64.3% allocated to the calciner reactor. In the ASU block, in addition to supplying oxygen for the calciner and the combustion chamber of the Allam cycle, nitrogen is produced at a rate of 260.75 ton/hr with 93.4 mol% purity, which can be marketed as a product of this integrated plant.

In the Allam cycle, exhaust gases from the combustor (St. 4) reach a flow rate of 422.1 ton/hr. By passing through the flash separator block, 11.65 ton/hr of liquid water with 99.8 mol% purity exits the cycle. After multi-stage compression of CO₂, flow is split into two streams (St. 12 and 14). St. 12, with a flow rate of 14.4 ton/hr and 98.5 mol% purity, is mixed with DAC-regenerated CO₂, resulting in a combined mass flow of 135.1 ton/hr with 98.1 mol% purity. The integration point of the Allam cycle and DAC unit is at a mixer (MIX-05) which is mixing two streams one at 150 bar and the other one at 120 bar. Final pressure and temperature of this block is 120 bar and 38.9°C respectively and CO₂ is in liquid phase ready for further sequestration and storage. Another aspect of this integration is the system's water recovery. Recovered water from the ASU and the Allam cycle helps reduce the plant's total water consumption. After accounting for water separation in the ASU flash separator, adsorbent unit (ADS), and flash separation in the Allam cycle, the net water demand for the DAC decreased to 523 ton/hr, resulting in a 1.51% reduction in overall demand. As mentioned earlier, primary advantage of integrating the Allam cycle is its capability to capture 100% of CO₂ without the need for post-combustion equipment and a regeneration

process. Power island of this simulation, in comparison with Zolfaghari et al. [35] and Keith et al. [31], emits 8.2% and 18.6% less CO₂, respectively. This CO₂ emission by the power island is presented in Fig10. In this presentation red bar shows CO₂ emission by Combined Cycle (C.C) proposed in the work of Keith et al. The blue bar presents a modified C.C proposed by Zolfaghari et al. As it shown this modification reduced emitted CO₂ by the Allam cycle. As shown in the research by Keith et al., the C.C. produced approximately 17.46 ton/hr of CO₂, while the modified C.C. in Zolfaghari et al.'s study produced 15.49 ton/hr. In C.C., although the power cycle's CO₂ emission rate is a factor, a portion of the solvent is also required to capture the exhaust gases from the cycle. In the case of the Allam cycle, this solvent flow rate is reduced to zero.

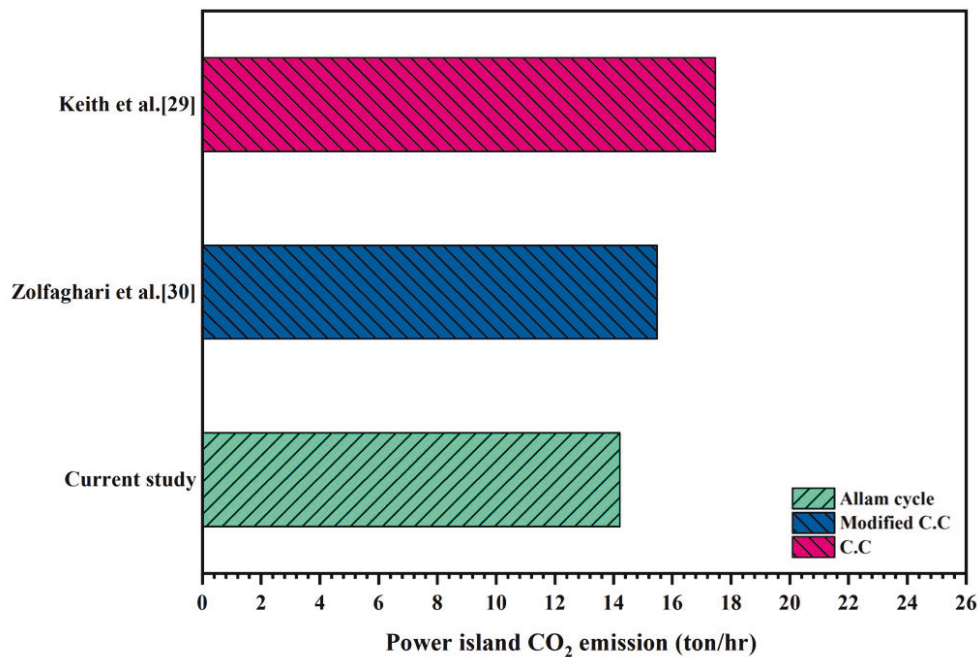


Fig. 8. CO₂ emission comparison of different power islands.

3.3 Energy demand

The highest electricity demand belongs to ASU compressors, accounting for 35.3% of the total, followed by the DAC compressors at 25.4%. Notably, 96.3% of the power is generated solely by the Allam cycle's turbine. Within the Allam cycle, the greatest energy demand is attributed to the CO₂ compressors. In this model, the ASU power demand for both the Allam cycle and DAC was 18.2 MW, which represents a 59.6% increase compared to Zolfaghari et al. [35] (11.4 MW) and a 36.8% increase compared to Keith et al. [31] (13.3 MW). Despite this higher energy demand, a greater amount of energy (57 MW) is produced with a lower mass flow rate of fuel compared to Zolfaghari et al and Keith et al. This highlights the impact of integrating the ASU with demand of both the Allam cycle and DAC blocks. Another aspect of the process involves thermal power analysis of the proposed systems. The mass flow rate of methane in the calciner reactor was adjusted to minimize fuel consumption and prevent additional fuel burning to achieve an adiabatic

reactor. Other reactors such as the Slaker are exothermic and release 60.7 MW of heat at 300°C to the surroundings. Table 8 presents all energy balances for thermal and electrical power consumed and produced in the system. Because of lack of modeling for air contactor power its demand has been set to 9.2 MW in order to report of Keith et al. The entire electrical power demand of the system is met by the Allam cycle, which generates electricity by burning fuel in the power island.

Table 8. Evaluation of the process energy balance.

Component	Power (MW)
Electrical power	
Allam fuel compressors	0.7
Allam CO ₂ compressors	8.8
Allam CO ₂ pumps	3.3
DAC pumps	0.2
DAC compressors	14.5
DAC air contactor	9.2
ASU compressors	20.1
ASU pump	0.2
ASU expander	-2.1
CO ₂ turbine	-54.9
Thermal power	
Allam combustor	0.00
Pellet reactor	-4.7
Slaker reactor	-60.7
Calciner	0.00
Heaters	157.9
Coolers	-102.4

Total heat requirement for heaters in the plant was 157.9 MW, while the heat rejected to the environment by coolers amounted to 102.4 MW. Further details on heaters and coolers can be found in Table 9. In this process integration and modification, 41.2 MW of heat is rejected by the DAC coolers. Of this, 20.91 MW—approximately half of the total heat rejection—comes from the intercoolers in the four-stage CO₂ compression, specifically from DAC.C-03 to DAC.C-06. The heat rejection for the Allam cycle amounts to 38.9 MW, which represents 37.9% of the total heat rejection. Among the heaters, the highest demand is for the (DAC.H-01) block, which vaporizes the stream’s water content, followed by (DAC.H-03), which raises its temperature to 300°C. This stream is a mixture of 0.82 % mol water and 0.18% mol CaCO₃ which is coming from washer at 53.5°C. Together, these two heaters account for 89.2% of the total heat demand. Meanwhile, the highest cooling demand is for (DAC.C-02) with 15.6 MW, followed by (C-6) with 10.29 MW for the Allam cycle. Within the Allam cycle alone, 38% of the heat rejection occurs, while 21.8% attributed to the ASU block and 40.2% to DAC block. The DAC block accounts for the largest share of hot utilities at 98.8% and represents 40.2% of the cold utilities in the process. The table also presents findings on heat recovery through heat exchangers, illustrating that the Allam cycle effectively recovers 53.9% of the total heat exchanged in the process. The highest heat exchange

occurs in REC1 of the Allam cycle, recovering 51.8% of the total heat, followed by HE-3 in the DAC block, which recovers 12.7%.

Table 9. Results of hot and cold utilities and recovered heat.

Cold Utility	Heat (MW)	Hot Utility	Heat (MW)	Heat Recovery	Heat (MW)
C-1	0.39	ASU.H-01	1.95	COLLER2	0.22
C-2	7.18	DAC.H-01	15.06	DAC.HE-1	11.92
C-3	1.22	DAC.H-02	109.66	DAC.HE-2	17.22
C-4	5.47	DAC.H-03	31.27	DAC.HE-3	24.17
C-5	9.34			DAC.HE-4	6.55
C-6	10.29			DAC.HE-5	3.95
C-7	1.26			DAC.HE-6	1.02
C-8	2.17			REC1	98.85
C-9	1.56			REC2	4.10
ASU.C-01	2.09			ASU.HXE	22.94
ASU.C-02	3.87				
ASU.C-03	6.92				
ASU.C-04	7.09				
ASU.C-05	2.36				
DAC.C-01	4.69				
DAC.C-02	15.6				
DAC.C-03	3.92				
DAC.C-04	3.64				
DAC.C-05	4.32				
DAC.C-06	9.03				
Summation	102.41	-	157.94	-	190.94

3.4 Energy optimization

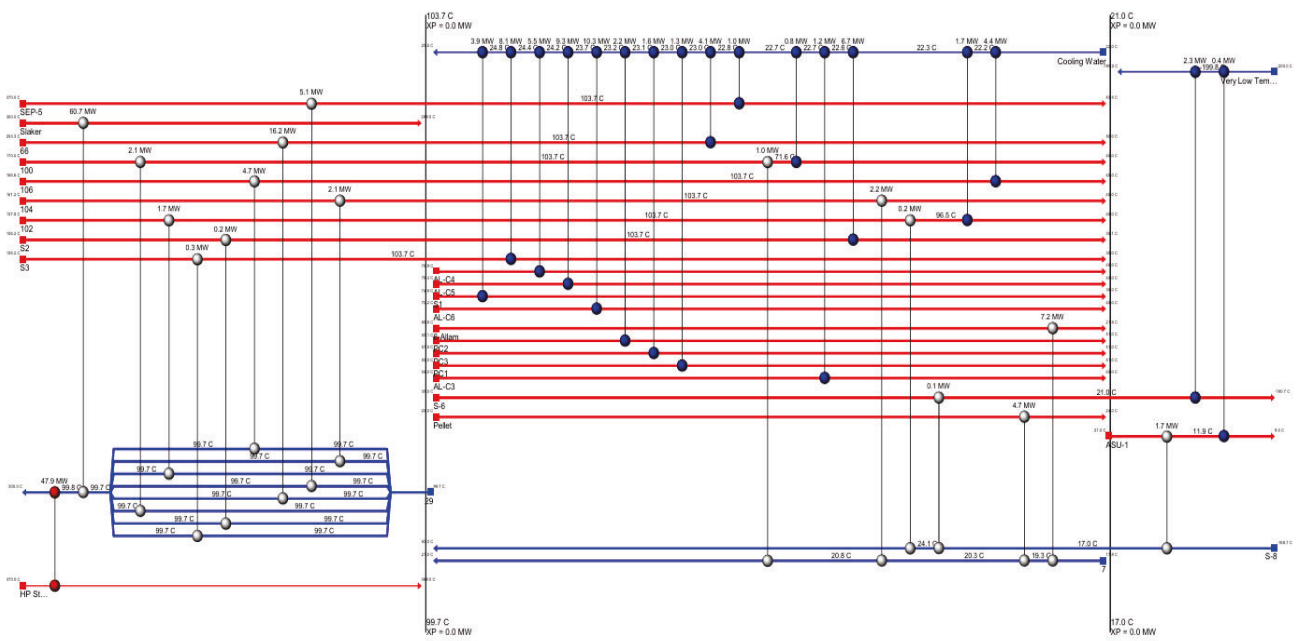
The pinch method analysis was utilized to minimize the plant's energy demand, specifically in the form of heat, thereby reducing reliance on external heat sources for cold streams. Economic considerations establish the minimum temperature approach for heat integration at 4°C, and the resulting grid diagram is depicted in Fig. 11. In this diagram, red dots represent external hot utilities, blue dots signify external cold utilities, and white dots denote heat exchangers. The integration process identifies two pinch points: one for the process pinch and another for the utility pinch. The streams are represented by blue color for cold streams and red color for hot streams. Following this design, the process's heat demand was reduced to 47.87 MW, achieving a 69.7% reduction, while heat rejection from hot streams decreased to 64.60 MW, a reduction of 36.9%. Overall, this integration recovered a total of 110.1 MW of heat through heat exchangers. The process is divided into two sections: above the pinch and below the pinch. The design of heat exchangers begins at the point where the process is most constrained, typically at the pinch point. As in Fig.11 is depicted most of the hot streams above the process pinch point (103.7°C) belong to DAC unit except streams S2 and S3. The phase change process occurs in the hot streams 66, S-

6, and AL-C6, as well as in the cold streams S-8 and 29. The coolers of the Allam cycle block operate below the process pinch temperature (103.7°C), meaning they do not contribute to reducing the heat demand above 100°C. The majority of the heat demand is tied to the phase change of water in the DAC.H-02 block, which occurs at 100°C. After the design is completed, the results need to be compared with the target values to assess the optimality of the design. Table 10 presents the results and targets as follows. According to [35], target levels are acceptable within a range below 10%.

Table 10. Comparison of designed and target values in the heat exchangers network.

	Target values	Current network	Deviation values (%)
Heating (MW)	47.87	47.87	0
Cooling (MW)	64.60	64.603	0.01
Number of heat exchangers	34	34	0
Total area (m ²)	3.7577×10^4	3.9576×10^4	5.32

As shown in Table 10, the highest deviation from the target value is 5.3%, which falls below the acceptable range. This deviation indicates that the proposed design of heat exchangers has been optimized using the Maximum Energy Recovery (MER) method and has successfully met the planned thermal energy demand.



3.5 Key performance indicators

This study disregarded the electricity supplied from the power grid, and instead focused on the plant's energy demands being met through fuel combustion. According to the calculations in Equation (5), the CO₂ capture mass flow rate reached 112.5 ton/hr, without any direct CO₂ emissions and with only the air CO₂ outlet from the DAC contactor. Equation (6) calculates a CO₂ removal efficiency of 0.75, indicating that the plant can capture 75% of the CO₂ from the atmosphere. The last KPI (Equation (4)) was evaluated under both general and optimized conditions. In the general case, no heat integration was implemented, whereas in the optimized scenario, heat integration was achieved through pinch analysis. The energy analysis results from this study and previous researches are presented in Table 11, with a focus on processes that utilize KOH as the absorption solution.

Table 11. Results of specific energy demand analysis for the proposed system.

Reference	Energy demand	
	Heat (kWh/kg _{CO₂})	Electricity (kWh/kg _{CO₂})
[31]	2.45	-
[31]	1.458	0.366
[31]	1.458	0.077
[35]	1.455	0.343
Present study	3.192	-
Present study (Optimized)	2.213	-

Keith's initial energy analysis [31] comprises three scenarios for meeting plant energy demand: The first scenario solely relies on natural gas, consuming 2.45 kWh/kg_{CO₂}. The second scenario involves 1.458 kWh/kg_{CO₂} from burning natural gas and 0.366 kWh/kg_{CO₂} from grid electricity. The third scenario excludes the CO₂ compression unit, resulting in 1.455 kWh/kg_{CO₂} from burning fuel and 0.077 kWh/kg_{CO₂} from electricity. Zolfaghari et al. [35] modified the plant's combined cycle, achieving 1.455 kWh/kg_{CO₂} from heat and 0.343 kWh/kg_{CO₂} from electricity. For this study the specific energy consumption for CO₂ capture, resulting in energy requirements of 11.49 MJ/kg_{CO₂} (3.192 kWh/kg_{CO₂}) and 7.97 MJ/kg_{CO₂} (2.213 MJ/kg_{CO₂}) for general and optimized case respectively. Compared to Keith's analysis, the general case had a 30.3% higher energy intensity, whereas the optimal case achieved an 9.66% reduction in the energy intensity.

4 Conclusion

DAC technology offered a viable approach for reducing atmospheric CO₂ concentrations, with anticipated advancements expected to lower both costs and energy demands. This study presented a comprehensive model that integrated HT-DAC using KOH with the S-CO₂ cycle, marking a significant contribution to carbon capture and energy optimization. The integration of these technologies represented a substantial advancement in the development of effective and efficient NETs. Several critical factors were investigated in this study, including: (i) the design of the ASU

to meet the demands of both the power cycle and the DAC cycle, (ii) performance evaluation of the plant utilizing the S-CO₂ cycle without relying on conventional gas and steam turbines, and (iii) energy optimizing through Pinch analysis method to reduce the system's energy consumption. Key findings from the study are as follows:

- Among the four different system configurations studied for feeding oxygen to the Allam cycle, the highest efficiency (55.5%) was achieved using oxygen pumping, compared to compressors which yielded an efficiency of 51.2%.
- The power island's CO₂ emissions were 14.21 ton/hr, which is 8.2% and 18.6% lower than those of the combined cycle and its modifications needed to fulfill DAC power requirements.
- The HT-DAC system captures 0.99 Mt of CO₂ annually, offering supporting applications in the beverage industry, synthetic fuel production, and underground storage. Notably, this integration also reduces water demand by 1.51%, further enhancing system performance.
- With a capture efficiency of 75%, the specific energy requirement for CO₂ capture was 11.49 MJ/kg_{CO₂} in the general case, which was reduced to 7.97 MJ/kg_{CO₂} (2.21 kWh/kg_{CO₂}) in the optimized case.
- Through optimization via pinch method analysis, the hot and cold utility requirements were reduced by 69.7% and 36.9%, respectively. Additionally, 110.1 MW of heat was recovered through the design of a heat exchangers networks.

References

1. Saray, J.A., A. Gharehghani, and D. Hosseinzadeh, *Towards sustainable energy Carriers: A solar and Wind-Based systems for green liquid hydrogen and ammonia production*. Energy Conversion and Management, 2024. **304**: p. 118215.
2. Agreement, P. *Paris agreement*. in *report of the conference of the parties to the United Nations framework convention on climate change (21st session, 2015: Paris)*. Retrived December. 2015. HeinOnline.
3. Ahbabi Saray, J. and M.M. Heyhat, *Multi-objective assessment of a DAPTC based on 4E analysis: Water-energy-environment nexus*. International Journal of Energy Research, 2022. **46**(15): p. 22541-22557.
4. Leonzio, G., et al., *Environmental performance of different sorbents used for direct air capture*. Sustainable Production and Consumption, 2022. **32**: p. 101-111.
5. Ahmadi, S., et al., *Design and evaluation of renewable energies-based multi-generation system for hydrogen production, freshwater and cooling*. Renewable Energy, 2022. **198**: p. 916-935.
6. Heyhat, M.M., et al., *Comparative assessment of direct absorption solar collector performance in different climates*. Scientific Reports, 2023. **13**(1): p. 21359.
7. Erans, M., et al., *Direct air capture: process technology, techno-economic and socio-political challenges*. Energy & Environmental Science, 2022. **15**(4): p. 1360-1405.
8. Ji, Y., et al., *Thermodynamic analysis on direct air capture for building air condition system: balance between adsorbent and refrigerant*. Energy and Built Environment, 2023. **4**(4): p. 399-407.
9. Abdullatif, Y.M., et al., *Optimizing chemisorption based direct air capture unit efficiency in HVAC systems: A study on the impact of DAC location and adsorption conditions as a response to the climate crisis and indoor air quality*. Energy Conversion and Management, 2023. **291**: p. 117280.

10. Rodríguez Hervás, G. and F. Petrakopoulou, *Exergoeconomic analysis of the allam cycle*. Energy & fuels, 2019. **33**(8): p. 7561-7568.
11. Xin, T., et al., *Process splitting analysis and thermodynamic optimization of the Allam cycle with turbine cooling and recompression modification*. Energy, 2024. **286**: p. 129458.
12. Xu, J., et al., *Perspective of S- CO2 power cycles*. Energy, 2019. **186**: p. 115831.
13. Isles, J., *Gearing up for a new supercritical CO2 power cycle system*. Gas Turbine World, 2014. **44**(6): p. 14-18.
14. Reale, F., *The Allam Cycle: A Review of Numerical Modeling Approaches*. Energies, 2023. **16**(22): p. 7678.
15. Colleoni, L., A. Sindoni, and S. Ravelli, *Comprehensive Thermodynamic Evaluation of the Natural Gas-Fired Allam Cycle at Full Load*. Energies, 2023. **16**(6): p. 2597.
16. Snæbjörnsdóttir, S.Ó., et al., *Carbon dioxide storage through mineral carbonation*. Nature Reviews Earth & Environment, 2020. **1**(2): p. 90-102.
17. Matter, J.M., et al., *Rapid carbon mineralization for permanent disposal of anthropogenic carbon dioxide emissions*. Science, 2016. **352**(6291): p. 1312-1314.
18. Prats-Salvado, E., et al., *Solar-Powered Direct Air Capture: Techno-Economic and Environmental Assessment*. Environmental Science & Technology, 2024.
19. Xu, H., et al., *A comprehensive review on direct air carbon capture (DAC) technology by adsorption: From fundamentals to applications*. Energy Conversion and Management, 2024. **322**: p. 119119.
20. Zhang, Z. and H. Xu, *Thermodynamic modeling on multi-stage vacuum-pressure swing adsorption (VPSA) for direct air carbon capture with extreme dilute carbon dioxide*. Energy, 2023. **276**: p. 127550.
21. Zhang, Z., et al., *Thermodynamics analysis of multi-stage temperature swing adsorption cycle for dilute CO2 capture, enrichment and purification*. Energy Conversion and Management, 2022. **265**: p. 115794.
22. Sanz-Pérez, E.S., et al., *Direct capture of CO2 from ambient air*. Chemical reviews, 2016. **116**(19): p. 11840-11876.
23. Lackner, K.S., *Capture of carbon dioxide from ambient air*. The European Physical Journal Special Topics, 2009. **176**(1): p. 93-106.
24. Agency, I.E., *Direct Air Capture*. 2022.
25. An, K., et al., *A comprehensive review on regeneration strategies for direct air capture*. Journal of CO2 Utilization, 2023. **76**: p. 102587.
26. Zeman, F.S. and K.S. Lackner, *Capturing carbon dioxide directly from the atmosphere*. World Resource Review, 2004. **16**(2): p. 157-172.
27. Baciocchi, R., G. Storti, and M. Mazzotti, *Process design and energy requirements for the capture of carbon dioxide from air*. Chemical Engineering and Processing: Process Intensification, 2006. **45**(12): p. 1047-1058.
28. Mahmoudkhani, M. and D.W. Keith, *Low-energy sodium hydroxide recovery for CO2 capture from atmospheric air—Thermodynamic analysis*. International Journal of Greenhouse Gas Control, 2009. **3**(4): p. 376-384.
29. Socolow, R., et al., *Direct air capture of CO2 with chemicals: a technology assessment for the APS Panel on Public Affairs*. 2011.
30. Mahmoudkhani, M., et al., *Low energy packed tower and caustic recovery for direct capture of CO2 from air*. Energy Procedia, 2009. **1**(1): p. 1535-1542.
31. Keith, D.W., et al., *A process for capturing CO2 from the atmosphere*. Joule, 2018. **2**(8): p. 1573-1594.
32. Sabatino, F., et al., *Evaluation of a direct air capture process combining wet scrubbing and bipolar membrane electrodialysis*. Industrial & Engineering Chemistry Research, 2020. **59**(15): p. 7007-7020.

33. Marchese, M., et al., *CO₂ from direct air capture as carbon feedstock for Fischer-Tropsch chemicals and fuels: Energy and economic analysis*. Journal of CO₂ Utilization, 2021. **46**: p. 101487.
34. An, K., A. Farooqui, and S.T. McCoy, *The impact of climate on solvent-based direct air capture systems*. Applied Energy, 2022. **325**: p. 119895.
35. Zolfaghari, Z., et al., *Simulation of carbon dioxide direct air capture plant using potassium hydroxide aqueous Solution: Energy optimization and CO₂ purity enhancement*. Energy Conversion and Management: X, 2024. **21**: p. 100489.
36. Allam, R.J., et al., *High efficiency and low cost of electricity generation from fossil fuels while eliminating atmospheric emissions, including carbon dioxide*. Energy Procedia, 2013. **37**: p. 1135-1149.
37. Zhu, Z., et al., *A modified Allam cycle without compressors realizing efficient power generation with peak load shifting and CO₂ capture*. Energy, 2019. **174**: p. 478-487.
38. Sleiti, A.K. and W.A. Al-Ammari, *Energy and exergy analyses of novel supercritical CO₂ Brayton cycles driven by direct oxy-fuel combustor*. Fuel, 2021. **294**: p. 120557.
39. Sleiti, A.K. and W.A. Al-Ammari, *Off-design performance analysis of combined CSP power and direct oxy-combustion supercritical carbon dioxide cycles*. Renewable Energy, 2021. **180**: p. 14-29.
40. Haseli, Y. and N.S. Sifat, *Performance modeling of Allam cycle integrated with a cryogenic air separation process*. Computers & Chemical Engineering, 2021. **148**: p. 107263.
41. Fernandes, D., et al., *Process and carbon footprint analyses of the Allam cycle power plant integrated with an air separation unit*. Clean technologies, 2019. **1**(1): p. 22.
42. Scaccabarozzi, R., M. Gatti, and E. Martelli, *Thermodynamic analysis and numerical optimization of the NET Power oxy-combustion cycle*. Applied energy, 2016. **178**: p. 505-526.
43. Scaccabarozzi, R., et al., *Solid oxide semi-closed CO₂ cycle: A hybrid power cycle with 75% net efficiency and zero emissions*. Applied Energy, 2021. **290**: p. 116711.
44. Chan, W., et al., *Exergoeconomic analysis and optimization of the Allam cycle with liquefied natural gas cold exergy utilization*. Energy Conversion and Management, 2021. **235**: p. 113972.
45. Wang, S., et al., *New Conceptual Design of an Integrated Allam-Cycle Power Complex Coupling Air Separation Unit and Ammonia Plant*. Industrial & Engineering Chemistry Research, 2021. **60**(49): p. 18007-18017.
46. Xu, C., et al., *Thermodynamic analysis of a novel biomass polygeneration system for ammonia synthesis and power generation using Allam power cycle*. Energy Conversion and Management, 2021. **247**: p. 114746.
47. Xin, T., et al., *Thermodynamic analysis of a novel zero carbon emission coal-based polygeneration system incorporating methanol synthesis and Allam power cycle*. Energy Conversion and Management, 2021. **244**: p. 114441.
48. Ioannou, I., et al., *Economic and Environmental Performance of an Integrated CO₂ Refinery*. ACS Sustainable Chemistry & Engineering, 2023. **11**(5): p. 1949-1961.
49. Borhani, T.N. and M. Wang, *Role of solvents in CO₂ capture processes: The review of selection and design methods*. Renewable and Sustainable Energy Reviews, 2019. **114**: p. 109299.
50. Ahamed, M., et al., *Comparative assessment of sCO₂ cycles, optimal ORC, and thermoelectric generators for exhaust waste heat recovery applications from heavy-duty diesel engines*. Energies, 2023. **16**(11): p. 4339.
51. Sifat, N.S. and Y. Haseli. *Thermodynamic modeling of Allam cycle*. in *ASME International Mechanical Engineering Congress and Exposition*. 2018. American Society of Mechanical Engineers.
52. Sleiti, A.K., et al., *Direct-fired oxy-combustion supercritical-CO₂ power cycle with novel preheating configurations-thermodynamic and exergoeconomic analyses*. Energy, 2021. **226**: p. 120441.